Semiconductor Physics, Quantum Electronics & Optoelectronics, 2024. V. 27, No 1. P. 095-108.

Optics

The conductivity effect of the top coating on optical properties of thin Cu(Ag)-layered structures

P.O. Kovanzhi[1*], I.H. Hyrman[1], V.G. Kravets[2], O.S. Kondratenko[3], L.V. Poperenko[1]

[1]*Taras Shevchenko National University of Kyiv, 60, Volodymyrska str., 01033 Kyiv, Ukraine*
[2]*Department of Physics and Astronomy, University of Manchester, Oxford Road, Manchester M13 9PL, UK*
[3]*V. Lashkaryov Institute of Semiconductor Physics, NAS of Ukraine, 45, prosp. Nauky, 03680 Kyiv, Ukraine*
[*]*Corresponding author e-mail: petrk1695@gmail.com*

Abstract. This study examines the optical properties of thin Cu (Ag)-layered structures covered with protective layers based on graphene, titanium (TiO_2), or aluminium (Al_2O_3) oxides. The objective is to investigate the impact of these coatings on the optical behaviors of underlying metallic layers, specifically in the spectral range of excitation of surface plasmon resonances. Combining the methods of spectroreflectometry and spectro-ellipsometry was used to analyze the optical characteristics of the hybrid metal-oxide-graphene films. The study shows that graphene, due to its exceptional electrical conductivity and unique optoelectronic properties, significantly modifies the optical behavior of investigated structures. It includes notable changes in refractive and absorption indices, and optical conductivity indicating potential for enhancing light-matter interactions in plasmonic-graphene layered structures with the aim to apply as biosensor. It is important that addition of TiO_2 and Al_2O_3 layers has also strong effects on the optical properties, which are relevant to their respective applications in the fields of optoelectronics and microelectronics. Employing the effective medium approximation and the Tauc–Lorentz model promotes deeper understanding the interplay between interband and intraband electronic transitions at the nanoscale level. It was revealed that the layer thickness of constituted materials and their individual dielectric functions together with addition of a graphene monolayer commit the significance for altering the optical properties of hybrid layered structures. The obtained results are important for the fields of plasmonics and nanotechnology, providing insights for designing sensors and devices with improved optical characteristics.

Keywords: thin-film optics, graphene coatings, spectroellipsometry, plasmonics, biosensing applications.

https://doi.org/10.15407/spqeo27.01.095
PACS 07.60.Fs, 68.65.Pq, 73.20.Mf, 78.67.Wj

Manuscript received 24.01.24; revised version received 10.02.24; accepted for publication 28.02.24; published online 12.03.24.

1. Introduction

Noble metals such as Cu and Ag have considerable potential for application in plasmonics. One of important limitation factor to use their decent plasmonic behaviours is the oxidizing with time and in liquid environments. To protect the Cu and Ag metallic layers from oxidation in air/liquid surrounding, they are often covered with a dielectric layer. Recently, it was shown that Cu(Ag) based plasmonic nanostructures can be used as effective and sensitive biosensors, if their surface is covered with an additional oxide layer and graphene monolayer [1].

Usualy, plasmonic biosensors are designed to monitor and analyze interactions between a target analyte derived from biological samples (such as antigens, proteins, peptides, DNA, and RNA segments) and its selectively immobilized receptor on a surface (such as antibodies, proteins and peptides) [2]. Traditional biosensing methods rely on fluorescence or radio labels to detect biomolecular binding. However, this labeling process introduces additional time, escalates costs and may result in false negative signals by obstructing the binding site [3, 4]. As functionalized layers in plasmonic biosensors, thin Au or graphene monolayer are the best

choices [3, 5]. Such biosensors have long history in applying Au functionalized layers and only decade in using of graphene [6–8].

The extraordinary optical, electrical, and physical properties of graphene make it an ideally-like top layer for various samples, especially in the realm of biosensing [6]. Graphene is a two-dimensional carbon sheet with a single-atom thickness and a hexagonal honeycomb lattice structure. Graphene's high conductivity and its status as a two-dimensional material with massless Dirac fermions contribute to its unparalleled sensitivity in biosensing applications [9]. Moreover, graphene is an exceptional electrical conductor that contributes to the immobilization of biomolecules and enhances electronic and ionic transportation capabilities in electrochemical sensors. Additionally, the optoelectronic properties of graphene, such as its capacity for quenching fluorescent molecules across a wide range of frequencies, open up possibilities for innovative sensing applications that employ Förster and fluorescence resonance energy transfer (FRET) as well as SERS-based sensors [10]. These sensors can be applied in various fields, such as biomedical diagnostics, environmental monitoring and chemical detection [11, 12].

From this point of view, we suggest to use graphene/TiO_2(Al_2O_3) as a material of topping layer for prototype heterostructure of biosensor. Note that TiO_2-coated materials demonstrated photocatalytic cleaning effects by efficiently breaking down organic molecules like stearic acid into CO_2 utilizing UV light [13]. This attribute has enabled the creation of self-cleaning surfaces. Due to their wide bandgap, TiO_2 requires an extensive amount of energy for excitation, ultimately necessitating the utilization of UV light for optimal energy transfer [14, 15]. Aluminum oxide (Al_2O_3) thin films have various fascinating characteristics, such as high optical transparency, robust resistance to abrasion and corrosion, substantial chemical and thermal stability, and a broad bandgap [16, 17]. Due to these unique properties, they are widely used in optoelectronics and microelectronic devices as insulating layers, durable protective coatings and surface passivation agents [18].

In this study, we have examined the effects of top coatings of graphene/TiO_2(Al_2O_3) on the optical characteristics of nanostructured thin Cu (Ag) films. Spectroreflectometry and spectroellipsometry methods were used to determine reflection coefficients and azimuths of restored linear polarization in *p*-polarized light at a constant angle of incidence (70°). The goal of this study was to investigate the effect of adding layers of graphene, titanium oxide and aluminum oxide to thin copper Cu or silver Ag films on their optical properties, including refractive index *n*, absorption index κ, as well as the real ε_1 and imaginary part ε_2 of the dielectric function and optical conductivity.

These complex optical properties were determined from spectroellipsometric measurements at the principal angle of incidence with high precision. The analysis of the obtained data was provided by using two methods: the effective medium approximation (EMA) and the Tauc–Lorenz model for each layer of the heterostructure (see in details, Supplement Information). Note, that the effective real and imaginary part of the dielectric function plays an important role in determining the dispersion properties of surface plasmon-polariton (SPP), spectral position and depth of the surface plasmonic resonance (SPR) curve. EMA allows one to describe the optical properties of few layer structures with dielectric and dielectric-graphene layers of small thickness. We consider bilayer (three-layer) stacks as single homogenize layer. Indeed, the entire multilayer stack can be treated as a single effective medium, where small phase shifts are present between neighbouring layers. This assumption is plausible for top dielectric or dielectric/graphene layer that is much thinner (~7 nm) than the probing wavelength and skin depth of noble metal (< 25 nm). It was shown that the effective dielectric functions, for these nanostructures are the smooth monotonic functions, which can be fairly approximated by Drude permittivity in the part of visible and the IR ranges and, what is more important, within the range of SPR excitation. The effective dielectric functions can be employed for simulation of SPR by using the Fresnel approach [19]. It is worth to note that the reality is more complicated and SPR in the Cu(Ag)/dielectric/graphene hybrid nanostructures occur in the spectral range where present is the contribution into optical behaviour not only from intraband electron transition but also from the interband ones. We used the Tauc–Lorentz model to evaluate spectral singularities in the density of electron states associated with interband electron transitions and absorption features of plasmonic dielectric-graphene nanostructures [20]. Suggested modeling carries out to systematically optimizing the parameters for the Cu(Ag)/dielectric/graphene hybrid nanostructures, in order to balance the optical absorption efficiencies and the electron losses at the plasmonic resonance condition.

2. Preparation of samples and the method of measurements

2.1. Sample preparation

The electron-beam deposition method was used to prepare thin metal Cu(Ag) films. The deposition rate was precisely controlled at the level of approximately 1.0 $Å \cdot s^{-1}$ by using a calibrated quartz microbalance. The base pressure was maintained at $1.0 \cdot 10^{-6}$ Torr [1, 4]. An adhesive layer is formed by depositing the thin Cr coating on clean glass surfaces by using electron-beam evaporation. To prevent oxidation of Cu or Ag plasmonic layers, the dielectric layer made of Al_2O_3 (TiO_2) was also deposited using electron-beam evaporation without breaking the vacuum between the Ag (Cu) and dielectric layer depositions. A multi-step procedure including the transfer of a single-layer graphene onto a bilayer nanostructure was used to create Cu(Ag)/graphene/TiO_2(Al_2O_3) samples. The process of transferring CVD graphene involves the following steps:

(i) To provide structural support, the Cu foil substrate was covered with a monolayer of graphene acquired from 2D Semiconductors Company. This monolayer was prepared using spin-coating with a polymethyl methacrylate (PMMA) resist.
(ii) The copper substrate was etched in an ammonium persulfate solution, which led to separation of a floating membrane, then it was cleaned in deionized water. Subsequently, the PMMA/graphene films on a specific type of adhesive (*e.g.*, Scotch) to facilitate the transfer process.
(iii) The resulting monolayer of graphene was transferred onto the Cu(Ag)/structure by employing the standard wet-transfer technique as described in [7, 8].
(iv) Finally, after an overnight drying period, the PMMA layer was removed by immersion in acetone.

2.2. Sample measurements

The optical reflection spectra were measured using the J.A. Woollam M-2000F variable angle spectroscopic ellipsometer within the wavelength range 245 up to 1690 nm and the angle of incidence range 45 up to 90° [21, 22]. The optical properties of Cu(Ag)/TiO_2(Al_2O_3)/graphene samples were also investigated using a Semilab SE-2000 spectroscopic ellipsometer, as described in [23]. Spectroscopic ellipsometry (SE) is a non-contact and non-destructive optical analytical technique used to evaluation of the optical properties of large-area thin films. This includes the refractive index *n* and extinction coefficient *k* with high precision and sensitivity. SE is a powerful optical tool that records the polarization change of incident light reflected from a flat surface. SE measures both the amplitude and phase variations of reflected light. From the measurements, ellipsometric angles ψ and Δ main ellipsometric equation can be defined as $\rho = r_p / r_s = \tan\psi \exp(i\Delta)$, where ρ denotes the complex reflection ratio. ψ and Δ are related to the amplitude and phase differences between *p*- and *s*-polarized light [24, 25]. Fig. 1 shows the schematic of ellipsometric measurements.

Semilab SE-2000 allows one to carry out the measurements in the high-resolution mode at the wavelengths ranging from 275 to 2100 nm. Signal acquisition was achieved using single-point detectors. As a result, we obtained, the phase shift Δ(λ) between the *p*- and *s*-components of the polarization vector and the azimuth ψ(λ) of the restore linear polarization for our samples

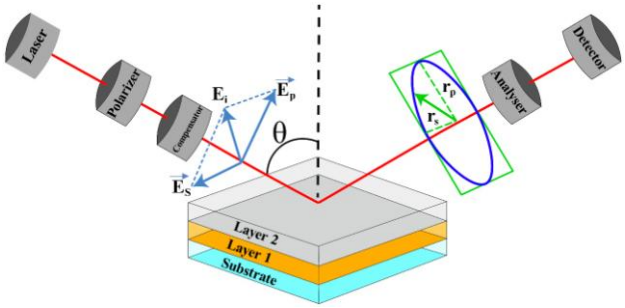

Fig. 1. Schematic of the Semilab SE-2000 optical configuration.

at a constant value of the light incidence angle (70°). These analyses allowed us to characterize and understand the optical behavior of the studied samples across a broad spectral range [26].

Besides, the spectroellipsometry as well as spectro-reflectometry for *p*-polarized light measurements within a shorter spectral interval in the visible range were also fulfilled at various angles of light incidence onto the samples to find clearly the presence of surface plasmon resonance phenomena in them.

3. Experimental results and discussion

For this study, we chose the samples presented in Table 1.

From ellipsometric measurements, we extracted optical properties of the investigated samples, including the refractive index *n*, absorption index κ (Fig. 2), as well as the real ε_1 and imaginary ε_2 parts of the dielectric function (Fig. 3).

In Table 1, we gathered all measured samples that can be selected into three different groups.

Group 1. The study focuses on the impact of copper layer thickness and addition of the graphene as a top layer on the optical properties.

As one can see in Fig. 2, a typical feature of the obtained dependences is located in the vicinity of wavelength λ = 550 nm, where the intraband electronic transitions start to prevail over the interband ones. The κ values increase whereas λ rises, which indicates growth of absorption in the near infrared range as compared to that in the visible range. The presence of weak minima in the visible range indicates resonant character of absorption in these samples due to interband electron transitions and may be also partially related to plasmonic excitation.

Table 1. Selected samples.

Cr(1.5nm)/Cu(43nm)	Cr(1.5nm)/Cu(40nm)/TiO_2(7–8nm)	Cr(1.0nm)/Ag(45nm)/TiO_2(7nm)
Cr(1.5nm)/Cu(43nm)/graphene	Cr(1.5nm)/Cu(40nm)/Al_2O_3(7nm)	Cr(1.5nm)/Ag(45nm)/Al_2O_3(7nm)
Cr(1.2nm)/Cu(55nm)/graphene		
Cr(3.5nm)/Cu(40nm)/Al_2O_3(7nm)/graphene		

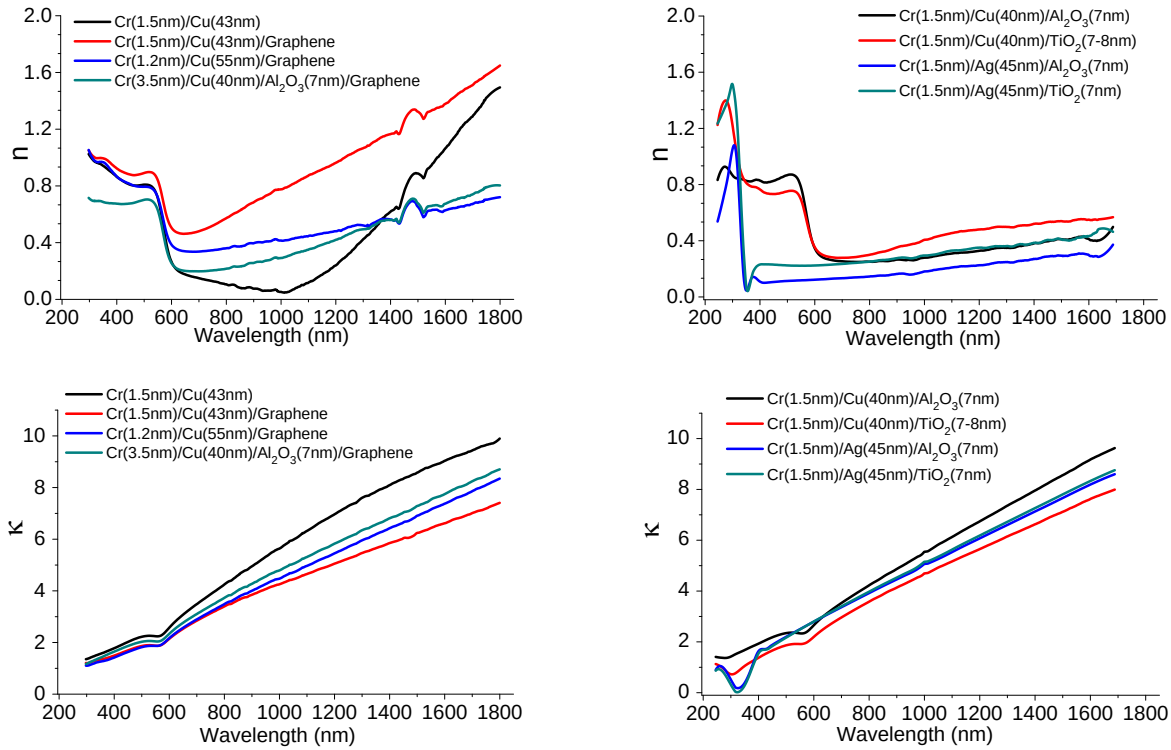

Fig. 2. The dependence of refractive index n and absorption index κ for Al_2O_3/TiO_2/graphene-Cu(Ag) structures on the light wavelength λ. (Color online)

It is clearly seen (Fig. 2) that addition of graphene to the Cu layers modifies both n and κ values, which is caused by the high graphene conductivity and changing the free electron density in hybrid nanostructures. Note that the high thickness of Cu layer covered with graphene monolayer also significantly alters the optical properties, which leads to a decrease in n and increase in κ (Fig. 2). Addition of graphene for Cu-based film resulted in rising the magnitude of n. It is interesting to note that the behavior of $n(\lambda)$ curves is similar for Cu-based layer with larger thickness (d = 55 nm) covered with graphene and sample with Cu (d = 40 nm), Al_2O_3 (d = 7 nm) and graphene.

In the three-layer Cu/Al_2O_3/graphene structure, optical properties are only slightly changed as compared to those of bilayer Cu/graphene (Figs 2 and 3) structure. This result gives evidence that additional interfaces associated with thin dielectric Al_2O_3 layer does not influence on the character of oscillations in the free electron ensemble. The oxide layer promotes to decrease the losses in Cu/Al_2O_3/graphene nanostructure and can affect the efficiency of plasmon excitation.

Furthermore, inspection of the n, κ and ε_1, ε_2 dependences (Figs 2 and 3) lead to conclusion that for Cu based hybrid nanostructures these functions can be approximated using the Drude permittivity in the red part of the visible and IR ranges.

The real part of dielectric function for Cu-based layered nanostructures becomes negative across a wide range of wavelengths from the visible to near-infrared ranges, which is characteristic for typical metals in this spectral range as shown in Fig. 3. It means that the condition for surface plasmon resonance (SPR) excitation (negative value of ε_1, and a small value of ε_2) can be established for these layered nanostructures at visible and near IR wavelengths.

Group 2. Evaluation of the effect of adding the TiO_2 and Al_2O_3 oxides on the top Cu layer.

Optical properties of bilayer structures $Cu/Al_2O_3(TiO_2)$ shows a pronounced feature around 600 nm in the spectral dependence of $n(\lambda)$ (Fig. 2). The presence of the above oxides provide smoothing of the real part of refraction index within the spectral interval 1000 up to 1700 nm, as compared to appropriate dependence for Cr(1.5 nm)/Cu(43 nm). Note that the TiO_2 coating layer promotes more pronounced growth of $n(\lambda)$ than the Al_2O_3 ones, probably due to its own higher refraction index which can lead to trap of light in results of internal reflection.

The values of absorptive part, κ, generally increases for all the investigated samples, while the wavelength rises and achieves the highest absorption in the case of sample covered with the Al_2O_3 thin layer. If to compare the optical properties of Cu(43 nm)/graphene and $Cu(40\text{ nm})/Al_2O_3(TiO_2)$ we can reveal the same increase of κ values over a broad wavelength range, especially in the near IR one (Fig. 2), which indicates the predominant contribution from free electrons of conductive Cu band.

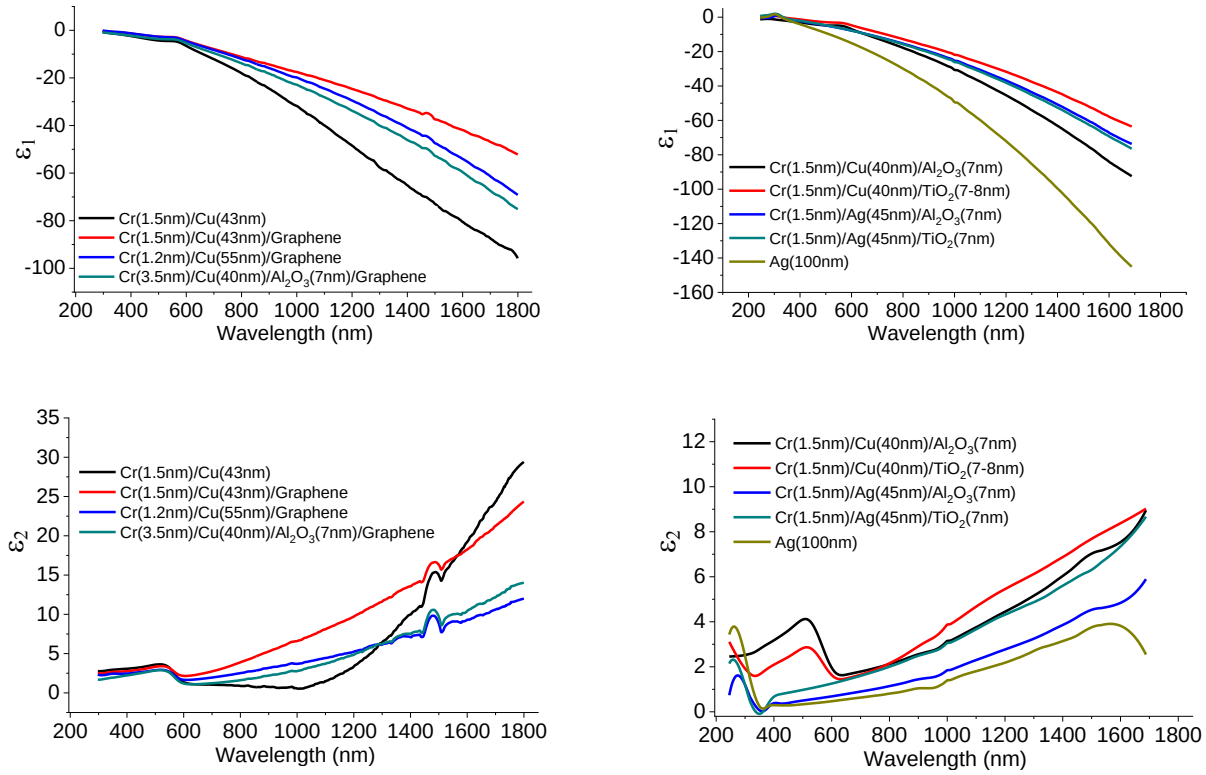

Fig. 3. The dependence of real ε_1 and imaginary ε_2 part of dielectric function for Al_2O_3/TiO_2/graphene-Cu(Ag) structures on the light wavelength λ. (Color online)

Fig. 3 presents dependences of the real ε_1 and imaginary parts ε_2 in the dielectric function for $Cu/Al_2O_3(TiO_2)$ layered structures, where the plasmonic-like behavior in the visible range of fabricated layers is underlined, because the negative values of ε_1 strongly rise and ε_2 is not large. Note that quality of Cu/Al_2O_3 layered structures as plasmonic material is preferable because of smaller ε_2 and larger ε_1 absolute values.

Group 3. Evaluation of effect of adding the TiO_2 and Al_2O_3 oxides on top Ag layer.

The measured complex refractive index of the $Cr/Ag/TiO_2$ and $Cr/Ag/Al_2O_3$ layered structures is shown in Fig. 2. It was found that the real part of refractive index *n* is larger for $Cr/Ag/TiO_2$ structure than for the $Cr/Ag/Al_2O_3$ one, while the absorptive part κ is approximately the same for both structures. We also see that both parts of the refractive index *n* and κ increase with increasing the wavelength within the range 400…1700 nm. The imaginary part of refractive index, κ, demonstrates higher values for the samples based on Ag than those on Cu plasmonic layer in red and near IR regions (compare Fig. 2). This tendency is related to larger contribution of inraband electron transitions in the layered $Cr/Ag/Al_2O_3(TiO_2)$ structures, as compared to that of $Cr/Cu/Al_2O_3(TiO_2)$. We can conclude that the spectral region corresponding to $\lambda > 500$ nm is highly sensitive to changes in the effective optical constants for plasmonic nanostructures. One pronounced extinction minimum appeared in κ and ε_2 curves in vicinity of $\lambda \approx 320$ nm (Figs 2 and 3). This dip can be associated with excitation of bulk plasmon resonance in $Cr/Ag/Al_2O_3(TiO_2)$ nanostructures. A bulk plasmon resonance, which occurs under conditions of $\varepsilon_1 \approx 0$ and small values of $\varepsilon_2 << 1$ (in other words, $n \approx \kappa$ and $\kappa << 1$) [27], is observed for Ag-based nanostructures but not for Cu ones (Fig. 3). In a pure silver layer, the plasmon resonance usually cannot be predicted by the free-electron theory and is shifted to longer wavelengths, in our measurements, in comparison to the case of $Cr/Ag/Al_2O_3(TiO_2)$ nanostructures (Fig. 3). Note that the strong dependence of ε_1 with increasing the wavelength for pure Ag layer (100 nm) demonstrates the Drude type of conductivity and high concentration of free electrons. Furthermore, addition of a thin dielectric layer on the top of Ag plasmonic layer strongly modifies the optical response and changes the free electron density. The Ag/TiO_2 layered nanostructure exhibits a higher absorption level than that of sample containing the Al_2O_3 layer. It can be related with the higher refractive index of TiO_2 as compared to that of alumina. We can assume that the dielectric layer with high real *n* can produce stronger screening effect for local electrical field at the metal-dielectric interface. These results are consistent with the recently published one [4], where high-performance surface plasmonic devices based on $Cu(Ag)/HfO_2$ was

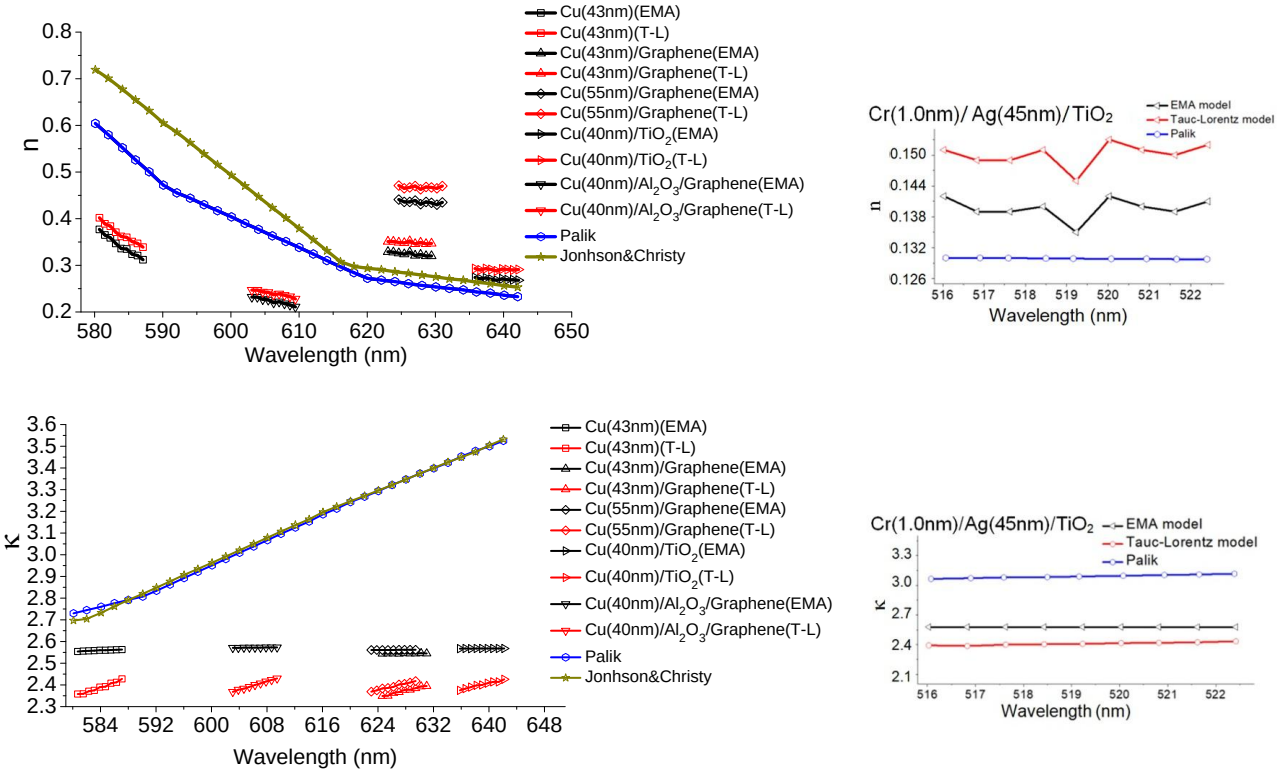

Fig. 4. The refractive index *n* and absorption coefficient κ for the effective medium models (EMA) and the Tauc–Lorentz model as a function of light wavelength λ. (Color online)

demonstrated due to enhancing the plasmonic resonance of pure Ag or Cu SPR by adding a high-refractive thin dielectric layer and graphene monolayer.

At the next step, we employed the effective medium approximation (EMA) for describing the experimental data of optical properties in the investigated samples. In this approximation, we replaced a multilayer sample with a homogeneous and continuous absorbing semi-infinite medium. EMA model was used in a limited narrow wavelength region, which is important from the viewpoint of observing excitation SPR and ellipsometric parameter $\cos\Delta = 0$. The latter condition is important, because it allows determining the ellipsometric characteristics Ψ and Δ with the highest possible experimental accuracy and consistently evaluating the complex refractive index also with the highest precision. Additionally, we have tested EMA for prediction of optical properties of complex multilayered systems that can be used in designing highly effective SPR-like sensors with required behaviour. To separate the contribution from interband and intraband electrons transition into resulting optical properties, the Tauc–Lorentz model has been used.

From ellipsometric dependences of Δ on the wavelength and angle of incidence, it was identified wherein the angle $\varphi = 70°$ is psevdo-Brewster angle for layered nanostructures. The refractive index *n* and absorption index κ were determined using the optical data of individual layers and their thicknesses by employing the formulas (10) and (11) in EMA (Fig. 4 and Table 2) (see Supplement Information).

Furthermore, the values of optical conductivity $\sigma = n^*\kappa^*\nu^*$ and reflection coefficient $R = \frac{(n-1)^2 + \kappa^2}{(n+1)^2 + \kappa^2}$ were calculated being based on extracted values of absorption κ and refractive indices *n* in the frame of EMA, Fig. 5 and Table 3 (see Supplement Information). In this figure, we also collected data for σ and *R* approximated by EMA and Tauc–Lorentz models and for comparison the literature data from Johnson's [27] and Palik's [28] works.

It was revealed that resulting complex refractive index (Fig. 4) is strongly influenced by the thickness of the noble metal layers, the presence of graphene, and the choice of dielectric materials. Importantly to note that EMA can be a generally reliable method for predicting the optical behavior of layered thin films in the region of SPR excitation. Comparison of the experimental data of the complex refractive index with approximated by EMA and Tauc–Lorentz models (Fig. 4) gives evidence that the sensitivity and precision of EMA exceed the Tauc–Lorentz approach, which coincides with the conclusion of previous study [29]. Using highly precise values of *n* and κ obtained through EMA, we calculated the reflection coefficients that are presented in Table 3.

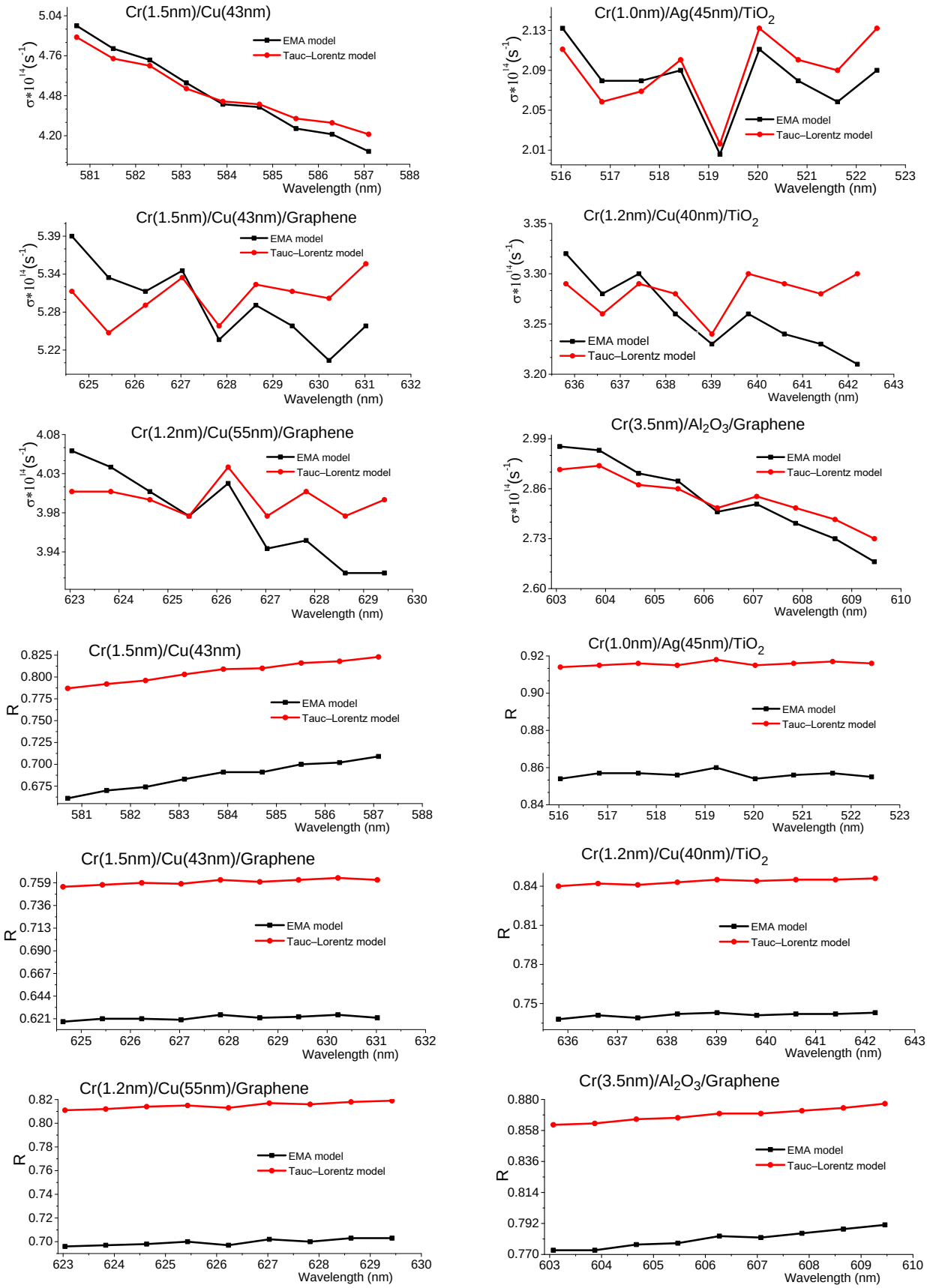

Fig. 5. The optical conductivity σ and reflection index *R* for the effective medium models (EMA) and the Tauc–Lorentz model as a function of light wavelength λ. (Color online)

The reflectivity $R(\lambda)$ and optical conductivity $\sigma(\lambda)$ of different Cu(Ag)/Al_2O_3(TiO_2)/graphene nanostructures are shown in Fig. 5. Inspection of the reflectivity $R(\lambda)$ for these nanostructures shows that for both types of multilayers $R(\lambda)$ are slightly increasing monotonic functions *versus* wavelength in the green-to-red spectral region. Behavior of the $\sigma(\lambda)$ is more complicated: it reaches the minimum at λ_{min} and then for $\lambda > \lambda_{min}$ grows. Covering with graphene the Cu(Ag)/Al_2O_3(TiO_2) bilayers reduces optical conductivity $\sigma(\lambda)$ in the visible region, which is indicative of lowered electron collisions [4, 27]. In the vicinity of minima $\sigma(\lambda_{min})$ for the investigated nanostructures, we can expect availability of the strongest singularities in SPP excitation, according to our recent work [4]. Being based on the dependences of $\sigma(\lambda)$ in the visible region, we can assume that the silver-dielectric-graphene hybrid thin layers possess higher quality of plasmon resonances than copper thin layers (compare Fig. 5: the dippiest minima and narrower half widths of SPR minima) due to smaller values of $\sigma(\lambda)$ and higher absolute values of ε_1 (Fig. 3). This highest quality SPRs of the silver-based nanostructures might promote their applications in the visible and near IR as biosensors.

From the viewpoint of electron band structure in Cu-based systems, interband transitions begin at about 600 nm; in Ag-based, at about 350 nm [28, 27]. It means that for Ag-based nanostructures the Drude theory for free electrons is expected to extend to the ultraviolet region, and consequently there arose a possibility of occurrence of SPRs in such broad spectral range. Modeling of the optical data for these two Ag(Cu)-based nanostructures by using EMA and Tauc–Lorentz approaches allows us to evaluate the band effects into the electron-electron interaction in Cu-based nanostructures in comparison of ideally free Drude-like electrons for Ag-based in the range of SPR. The interband electron transitions for Cu/Al_2O_3(TiO_2)/graphene layered structures was modeled using the Tauc–Lorentz approach [20] This model satisfactory describes optical properties of Cu/Al_2O_3(TiO_2)/graphene layered structures near the edges between interband and intraband electron transitions.

We covered plasmonic metals Cu and Ag with high-index dielectrics Al_2O_3 or TiO_2 and showed that these nanostructures can exhibit the enhanced surface absorption in the region of SPR existence. These high-refractive index dielectrics Al_2O_3 or TiO_2 cause decreasing the potential barriers (work function) of metal and, as a result, enhancing the number of electrons spilled from metal Cu and Ag into dielectrics [30, 31]. In addition, electron transfer due to the work function difference between dielectric layers and metals Cu (Ag) can promote a large electric field enhancement at the sensing interface and thus leading to higher sensitivity in the case of biosensor applications [1]. It is worth noting that, for example, the work function of Cu (~5.22 eV) [32] is higher than that of dielectrics Al_2O_3 (2.73 eV) and TiO_2 (2.1 eV) [31]. Effect of exchanging with electrons between bottom metals and top layers can be enhanced, if use the highly conductive graphene monolayer. The dimension scale of these electron transfers extends beyond the Thomas–Fermi (TF) screening length (the characteristic length $L_c = v_F/\omega$, where v_F is the Fermi velocity of electrons and ω is a light frequency). For standard values of about $v_F \sim 1.4 \cdot 10^6$ m/s, the resulting wavevector mismatch is on the scale of $\Delta\kappa \sim L_c^{-1}$, and it is about 2 nm^{-1} for noble metals at 600 nm, and it is much larger than the wavevector of the electromagnetic wave [33]. This process is insignificant at a metal-low-index refractive interface (for example, SiO_2) due to the high barrier, however, it could be large at a metal-high-index refractive interface (Al_2O_3, TiO_2), which was fabricated in this study, and could lead to intensified energy of surface plasmon and narrowed absorption spectrum [30].

In this study, it was shown that interaction between incident light and electron systems can be successfully described by convenient EMA despite the complex resulting electron band structures of Cu(Ag)/Al_2O_3(TiO_2)/graphene hybrid systems, in which the contributions exist from both classical and quantum effects (finite-size quantum effects, in particular the non-locality of the electron response [30]). Our results on the Cu(Ag)/Al_2O_3(TiO_2)/graphene layered structures indicate that the real part of the effective dielectric function $\varepsilon_1(\lambda)$ and optical conductivity $\sigma(\lambda)$ generally follow effective medium approach and the strongest SPR occurs at higher values of $\varepsilon_1(\lambda_{SPR})$ and the lower ones of $\sigma(\lambda_{SPR})$, which confirms and spreads the conclusion of [4].

4. Conclusions

Investigated in this work is the impact of upper coatings on the optical properties of thin Cu (Ag)-layered structures. Specifically, we focus on the influence of graphene, titanium oxide (TiO_2) and aluminum oxide (Al_2O_3) as top layers. The optical characteristics of the Cu(Ag)/Al_2O_3(TiO_2)/graphene layered structures were determined as being based on spectroellipsometric and spectroreflectometric measurements. It has been shown that the experimentally observed dependences of the ellipsometric characteristics and reflectivity of layered thin structures can be explained on the basis of EMA theory with introduction of effective complex refractive index and using the Fresnel reflection and transmission coefficients for effective thin layer on top of a glass substrate. We have found that the effective optical constants of investigated copper-dielectric or silver-dielectric based nanostructures determined through spectroscopic ellipsometry at the principle angle of incidence with the highest possible experimental accuracy and precision are highly sensitive to changes in the thickness of layers and optical properties of individual constituted layers.

Addition of graphene onto the top of $Cu(Ag)/Al_2O_3(TiO_2)$ bilayers significantly modifies the optical behavior, such as the refractive and absorption indices as well as the optical conductivity of investigated systems due to its unique optoelectronic properties.

The obtained results can find important implications in the field of designing effective plasmonic and optoelectronic devices provide insights into the engineering of high-performance plasmonic sensors and devices with improved optical characteristics.

Supplement Information

Theoretical prediction

Review the main models related to the topic of this paper.

Tauc–Lorentz model

The Tauc–Lorentz model, a robust model for assessing optics, is especially beneficial for disordered materials. This method is designed to simulate absorbance within the ultraviolet-visible (UV-Vis) spectrum, satisfying the necessity for a thorough comprehension of the optical features of materials, which manifest transparency at longer wavelengths but absorb at the UV-Vis spectrum [34].

At its core, the Tauc–Lorentz method combines the standard Lorentz oscillator model with a bandgap term proposed by Jellison and Modine [35] is generally used for amorphous materials, for example, Au thin layers.

The absorption band in the imaginary part of the dielectric function is defined as

$$\varepsilon_2 = \begin{cases} \dfrac{AE_0C\left(E-E_g\right)^2}{\left(E^2+E_0^2\right)^2+E^2C^2}\dfrac{1}{E} & E > E_g \\ 0 & E \le E_g \end{cases}, \quad (1)$$

the Tauc–Lorentz oscillator is denoted by A, C, and E_0, representing its amplitude, position, and broadening, respectively. The Tauc gap is represented by E_g.

In addition, the Tauc–Lorentz model adheres to the Tauc law for the imaginary part of a material dielectric function near its bandgap [36].

The versatility and adaptability of the Tauc–Lorentz model render it a valuable tool in the realm of materials science, notably for assessing and comprehending the optical characteristics of amorphous metal [37].

Effective medium model (EMA)

The effective medium approximation (EMA) is a prevalent theoretical method in spectroscopic ellipsometry for modeling optical properties of thin films with including their surface roughness. Essentially, EMA streamlines the intricate, microscopically rough surface of a sample into a flat layer described by an effective dielectric function [38]. EMA excels in converting the intricate, microscopic surface irregularities into a more manageable and analyzable form. Thus, it streamlines the process of estimating the effective dielectric function of the rough surface layer, facilitating the analysis of material optical properties simultaneously maintaining a reasonable level of precision. In summary, the EMA model serves as a crucial tool for optical characterization, especially in spectroscopic ellipsometry. It fulfills a significant role in comprehending and interpreting the intricate light interactions with rugged surfaces [39, 40].

The effective medium approximation, similar to the coherent potential approximation in solid state theory, is one of the basic approximations for elucidating the effective parameters of highly inhomogeneous composite media [41].

Initially proposed by Bruggeman [42], this model is aimed at delineating effective parameters within media featuring macroscopic inclusions.

This approximation method is particularly valuable when describing complex composite media exhibiting negative effective dielectric and/or magnetic function. However, while the volume ratios provide crucial insights into these effective parameters, the structural distribution of the media components significantly influences them. It's important to note that these volume components only offer a scope of effective parameters, which can be further refined, if additional structural details of the medium are available. In essence, understanding the structural intricacies plays a pivotal role in accurately determining the effective parameters of such composite materials.

The derivation of equations governing the effective medium involves the utilization of continuity equations stemming from the foundational principles of electromagnetism.

$$I = jS = \sigma_i E_{in}\, S \Rightarrow j = \sigma_i E_{in} \ . \quad (2)$$

In the effective medium approximation, the average polarization is zero $\left\langle \vec{p} \right\rangle = 0$:

$$\sigma_i = \sigma_{eff} \ . \quad (3)$$

A similar relationship for dielectric constant

$$X\frac{\varepsilon_1-\varepsilon_{eff}}{\varepsilon_1+2\varepsilon_{eff}}+\left(1-X\right)\frac{\varepsilon_0-\varepsilon_{eff}}{\varepsilon_0+2\varepsilon_{eff}}=0, \quad (4)$$

where

$$\sigma_{eff} = \varepsilon_\infty - \frac{4\pi i\sigma}{\omega} \ . \quad (5)$$

This approximation was called the Brueggemann approximation, with

$$\sigma_{eff} = \sigma^{EMA}. \quad (6)$$

Method of the principal angle

When incident linearly polarized light interacts with a polished metal surface, the resultant reflected light becomes elliptically polarized. The amplitudes of the *p*- and *s*-components of the reflected wave are related to the amplitudes of the incident wave by the Fresnel formulas:

$$\tilde{R}_s = -E_s \frac{\sin(\varphi - \tilde{\chi})}{\sin(\varphi + \tilde{\chi})} \qquad \tilde{R}_s = |R_s| e^{i\delta_s}, \tag{7}$$

$$\tilde{R}_p = E_p \frac{\mathrm{tg}(\varphi - \tilde{\chi})}{\mathrm{tg}(\varphi + \tilde{\chi})} \qquad \tilde{R}_p = |R_p| e^{i\delta_p}. \tag{8}$$

Upon reflection, the phase difference $\Delta = \delta p - \delta s$, in general, deviates from both zero and positive values. Thus, when linearly polarized light interacts with a metal surface, the resulting polarization generally adopts an elliptical nature:

$$\frac{\tilde{R}_p}{\tilde{R}_s} = \frac{|R_p|}{|R_s|} e^{i(\delta_p - \delta_s)} = \frac{|R_p|}{|R_s|} e^{i\Delta} = \mathrm{tg}\psi e^{i\Delta} = [\rho = \mathrm{tg}\psi] = \rho e^{i\Delta}. \tag{9}$$

The formulas for determining optical constants can be generalized. For this purpose, the angle of incidence is introduced $\varphi = \overline{\varphi}$, in which $\Delta = 90°$ and the maximal instrumental accuracy is reached. The primary angle of incidence is denoted as angle $\overline{\varphi}$, and it is accompanied by the main azimuth angle, which is angle $\overline{\psi}$ [43]. This yields the following result for optical constants *n* and κ:

$$n = \mathrm{tg}\overline{\varphi} \sin\overline{\varphi} \cos 2\overline{\psi}, \tag{10}$$

$$\kappa = \mathrm{tg}\overline{\varphi} \sin\overline{\varphi} \sin 2\overline{\psi}. \tag{11}$$

Table 2. Comparison of the results of the refractive index *n* and absorption coefficient κ for the EMA and Tauc–Lorentz (T–L) models.

Cr(1.5 nm)/Cu(43 nm)					Cr(1.5 nm)/Cu(43 nm)/graphene				
λ (nm)	*n* EMA	*n* T–L	κ EMA	κ T–L	λ (nm)	*n* EMA	*n* T–L	κ EMA	κ T–L
580.7	0.377	0.402	2.554	2.358	**624.6**	0.441	0.471	2.544	2.349
581.5	0.365	0.389	2.556	2.359	**625.4**	0.436	0.465	2.545	2.350
582.3	0.359	0.384	2.557	2.371	**626.2**	0.436	0.467	2.545	2.363
583.1	0.347	0.371	2.558	2.375	**627.0**	0.439	0.470	2.544	2.367
583.9	0.336	0.362	2.560	2.390	**627.8**	0.431	0.463	2.546	2.377
584.7	0.335	0.360	2.560	2.392	**628.6**	0.436	0.468	2.545	2.378
585.5	0.324	0.351	2.561	2.408	**629.4**	0.434	0.467	2.545	2.385
586.3	0.321	0.347	2.562	2.412	**630.2**	0.430	0.465	2.546	2.393
587.1	0.312	0.339	2.563	2.428	**631.0**	0.435	0.470	2.545	2.395

Cr(1.2 nm)/Cu(55 nm)/graphene					Cr(3.5 nm)/Cu(40 nm)/Al_2O_3(7 nm)/graphene				
λ (nm)	*n* EMA	*n* T–L	κ EMA	κ T–L	λ (nm)	*n* EMA	*n* T–L	κ EMA	κ T–L
623.0	0.329	0.351	2.561	2.369	**603.1**	0.232	0.247	2.571	2.368
623.8	0.328	0.351	2.561	2.375	**603.9**	0.232	0.247	2.571	2.378
624.6	0.326	0.349	2.561	2.384	**604.7**	0.227	0.243	2.572	2.383
625.4	0.324	0.348	2.561	2.386	**605.5**	0.226	0.242	2.572	2.391
626.2	0.328	0.352	2.561	2.391	**606.3**	0.220	0.237	2.572	2.400
627.0	0.321	0.346	2.562	2.402	**607.1**	0.222	0.239	2.572	2.407
627.8	0.323	0.349	2.562	2.405	**607.9**	0.218	0.236	2.573	2.416
628.6	0.320	0.346	2.562	2.411	**608.7**	0.215	0.233	2.573	2.423
629.4	0.320	0.347	2.562	2.418					

Table 2 continuation

Cr(1.5 nm)/Cu(40 nm)/TiO_2(7–8 nm)					Cr(1.0 nm)/Ag(45 nm)/TiO_2(7 nm)				
λ (nm)	*n* EMA	*n* T–L	κ EMA	κ T–L	λ (nm)	*n* EMA	*n* T–L	κ EMA	κ T–L
635.8	0.274	0.293	2.567	2.375	**516.0**	0.142	0.151	2.578	2.392
636.6	0.271	0.290	2.568	2.383	**516.8**	0.139	0.149	2.578	2.386
637.4	0.273	0.293	2.567	2.390	**517.6**	0.139	0.149	2.578	2.399
638.2	0.270	0.291	2.568	2.398	**518.4**	0.140	0.151	2.578	2.403
639.0	0.268	0.288	2.568	2.400	**519.2**	0.135	0.145	2.578	2.407
639.8	0.271	0.292	2.568	2.408	**520.0**	0.142	0.153	2.578	2.415
640.6	0.269	0.291	2.568	2.414	**520.8**	0.140	0.151	2.578	2.418
641.4	0.269	0.290	2.568	2.414	**521.6**	0.139	0.150	2.578	2.423

Table 3. Comparison of the results of the optical conductivity σ and reflection index *R* for the EMA and Tauc–Lorentz (T–L) models.

Cr(1.5 nm)/Cu(43 nm)					Cr(1.5 nm)/Cu(43 nm)/graphene				
λ (nm)	$\sigma\cdot10^{14}$ EMA	$\sigma\cdot10^{14}$ T–L	*R* EMA	*R* T–L	λ (nm)	$\sigma\cdot10^{14}$ EMA	$\sigma\cdot10^{14}$ T–L	*R* EMA	*R* T–L
580.7	4.97	4.89	0.661	0.787	**624.6**	5.39	5.31	0.618	0.755
581.5	4.81	4.74	0.670	0.792	**625.4**	5.33	5.25	0.621	0.757
582.3	4.73	4.69	0.674	0.796	**626.2**	5.31	5.29	0.621	0.759
583.1	4.57	4.53	0.683	0.803	**627.0**	5.34	5.33	0.620	0.758
583.9	4.42	4.44	0.691	0.809	**627.8**	5.24	5.26	0.625	0.762
584.7	4.40	4.42	0.691	0.810	**628.6**	5.29	5.32	0.622	0.760
585.5	4.25	4.32	0.700	0.816	**629.4**	5.26	5.31	0.623	0.762
586.3	4.21	4.29	0.702	0.818	**630.2**	5.21	5.30	0.625	0.764
587.1	4.09	4.21	0.709	0.823	**631.0**	5.26	5.35	0.622	0.762

Cr(1.2 nm)/Cu(55 nm)/graphene					Cr(3.5 nm)/Cu(40 nm)/Al_2O_3(7 nm)/graphene				
λ (nm)	$\sigma\cdot10^{14}$ EMA	$\sigma\cdot10^{14}$ T–L	*R* EMA	*R* T–L	λ (nm)	$\sigma\cdot10^{14}$ EMA	$\sigma\cdot10^{14}$ T–L	*R* EMA	*R* T–L
623.0	4.06	4.01	0.696	0.811	**603.1**	2.97	2.91	0.773	0.862
623.8	4.04	4.01	0.697	0.812	**603.9**	2.96	2.92	0.773	0.863
624.6	4.01	4.00	0.698	0.814	**604.7**	2.90	2.87	0.777	0.866
625.4	3.98	3.98	0.700	0.815	**605.5**	2.88	2.86	0.778	0.867
626.2	4.02	4.04	0.697	0.813	**606.3**	2.80	2.81	0.783	0.870
627.0	3.94	3.98	0.702	0.817	**607.1**	2.82	2.84	0.782	0.870
627.8	3.95	4.01	0.700	0.816	**607.9**	2.77	2.81	0.785	0.872
628.6	3.91	3.98	0.703	0.818	**608.7**	2.73	2.78	0.788	0.874
629.4	3.91	4.00	0.703	0.819					

Table 3 continuation

Cr(1.5 nm)/Cu(40 nm)/TiO_2(7–8 nm)					Cr(1.0 nm)/Ag(45 nm)/TiO_2(7 nm)				
λ (nm)	$\sigma\cdot10^{14}$ EMA	$\sigma\cdot10^{14}$ T–L	*R* EMA	*R* T–L	λ (nm)	$\sigma\cdot10^{14}$ EMA	$\sigma\cdot10^{14}$ T–L	*R* EMA	*R* T–L
635.8	3.32	3.29	0.738	0.840	**516.0**	2.13	2.11	0.854	0.914
636.6	3.28	3.26	0.741	0.842	**516.8**	2.08	2.06	0.857	0.915
637.4	3.30	3.29	0.739	0.841	**517.6**	2.08	2.07	0.857	0.916
638.2	3.26	3.28	0.742	0.843	**518.4**	2.09	2.10	0.856	0.915
639.0	3.23	3.24	0.743	0.845	**519.2**	2.01	2.02	0.860	0.918
639.8	3.26	3.30	0.741	0.844	**520.0**	2.11	2.13	0.854	0.915
640.6	3.24	3.29	0.742	0.845	**520.8**	2.08	2.10	0.856	0.916
641.4	3.23	3.28	0.742	0.845	**521.6**	2.06	2.09	0.857	0.917

References

1. Kravets V.G., Wu F., Yu T., Grigorenko A.N. Metal-dielectric-graphene hybrid heterostructures with enhanced surface plasmon resonance sensitivity based on amplitude and phase measurements. *Plasmonics*. 2022. **17**. P. 973–987. https://doi.org/10.1007/s11468-022-01594-y.
2. Hamza M.E., Othman M.A., Swillam M.A. Plasmonic biosensors: Review. *Biology*. 2022. **11**, No 5. P. 621. https://doi.org/10.3390/biology11050621.
3. Kabashin A.V., Kravets V.G., Grigorenko A.N. Label-free optical biosensing: going beyond the limits. *Chem. Soc. Rev*. 2023. **52**. P. 6554–6585. https://doi.org/10.1039/d3cs00155e.
4. Kravets V., Poperenko L., Kudryavtsev Yu., Kovanzhi P. Optical properties and electron characteristics of noble-metal-dielectric oxide nanostructures with covered graphene layer. *Opt. Mater.: X*. 2023. **19**. P. 100256. https://doi.org/10.1016/j.omx.2023.100256.
5. Wu L., Chu H.S., Koh W.S., Li E.P. Highly sensitive graphene biosensors based on surface plasmon resonance. *Opt. Express*. 2010. **18**, No 14. P. 14395–14400. https://doi.org/10.1364/OE.18.014395.
6. Li Z., Zhang W., Xing F. Graphene optical biosensors. *Int. J. Mol. Sci*. 2019. **20**, No 10. P. 2461. https://doi.org/10.3390/ijms20102461.
7. Kravets V.G., Wu F., Auton G.H. *et al*. Measurements of electrically tunable refractive index of MoS_2 monolayer and its usage in optical modulators. *NPJ 2D Mater. Appl*. 2019. **3**. P. 36. https://doi.org/10.1038/s41699-019-0119-1.
8. Kravets V.G., Jalil R., Kim Y.-J. *et al*. Graphene-protected copper and silver plasmonics. *Sci. Rept*. 2014. **4**. P. 5517. https://doi.org/10.1038/srep05517.
9. Geim A.K., Novoselov K.S. The rise of graphene. *Nature Materials*. 2007. **6**, Issue 3. P. 183–191. https://doi.org/10.1038/nmat1849.
10. Yin P.T., Kim T.-H., Choi J.-W., Lee K.-B. Prospects for graphene–nanoparticle-based hybrid sensors. *Phys. Chem. Chem. Phys*. 2013. **15**. P. 12785–12799. https://doi.org/10.1039/C3CP51901E.
11. Tiwari S.K., Sahoo S., Wang N., Huczko A. Graphene research and their outputs: Status and prospect. *J. Sci. - Adv. Mater. Dev*. 2020. **5**, No 1. P. 10–29. https://doi.org/10.1016/j.jsamd.2020.01.006.
12. Geim A.K. Graphene: Status and Prospects. *Science*. 2009. **324**(5934). P. 1530–1534. https://doi.org/10.1126/science.1158877.
13. Ziental D., Czarczynska-Goslinska B., Mlynarczyk D.T. *et al*. Titanium dioxide nanoparticles: Prospects and applications in medicine. *Nanomaterials* (Basel). 2020. **10**, No 2. P. 387. https://doi.org/10.3390/nano10020387.
14. Hashimoto K., Irie H., Fujishima A. TiO_2 photocatalysis: A historical overview and future prospects. *Jpn. J. Appl. Phys*. 2005. **44**. P. 8269. https://doi.org/10.1143/JJAP.44.8269.
15. Phukan P., Sahu P.P. High performance UV photodetector based on metal-semiconductor-metal structure using TiO_2-rGO composite. *Opt. Mater*. 2020. **109**. https://doi.org/10.1016/j.optmat.2020.110330.
16. Chen Y., Ud-Din R., Yang T. *et al.* Preparing and wear-resisting property of Al_2O_3/Cu composite material enhanced using novel *in situ* generated Al_2O_3 nanoparticles. *Materials* (Basel). 2023. **16**. No 13. P. 4819. https://doi.org/10.3390/ma16134819.
17. Gies M., Benz S.L., Pradja M.M. *et al.* Ultrathin Al_2O_3 protective layer to stabilize the electrochromic switching performance of amorphous WO_x thin films. *Adv. Mater. Interfaces*. 2023. **10**, No 12. https://doi.org/10.1002/admi.202202422.
18. Bouzbib M., El Marouani M., Sinkó K. Effect of various additives on aluminum oxide thin films prepared by dip coating, thermal behavior, kinetics and optical properties. *J. Eur. Opt. Soc. Rapid publ*. 2021. **17**. Art. No 25. https://doi.org/10.1186/s41476-021-00170-x.

19. Born M., Wolf E. *Principles of Optics*. Cambridge University Press, 1999.
20. Kravets V.G., Prorok V.V., Poperenko L.V., Shaykevich I.A. Ellipsometry and optical spectroscopy of low-dimensional family TMDs. *SPQEO*. 2017. **20**, No 3. P. 284–296. https://doi.org/10.15407/spqeo20.03.284.
21. Cusworth E., Kravets V.G., Grigorenko A.N. Topological darkness in optical heterostructures: Prediction and confirmation. *ACS Photonics*. 2023. **10**. P. 3715−3722. https://doi.org/10.1021/acsphotonics.3c00879.
22. Kuryoz P.Yu., Poperenko L.V., Kravets V.G. Correlation between dielectric constants and enhancement of surface plasmon resonances for thin gold films. *phys. status solidi* (*a*). 2013. **210**, No 11. P. 2445–2455. https://doi.org/10.1002/pssa.201329272.
23. Kondratenko O.S., Mamykin S.V., Lunko T.S. *et al*. Optical characterization of hybrid PEDOT:PSS/Si heterostructures by spectroscopic ellipsometry. *Mol. Cryst. Liquid Cryst*. 2021. **717**. https://doi.org/10.1080/15421406.2020.1860533.
24. Ma Y., Lu S., Dong X. *et al.* Optical parameters of graphene/MoS_2 van der Waals heterostructure investigated by spectroscopic ellipsometry. *Appl. Surf. Sci*. 2022. **599**. https://doi.org/10.1016/j.apsusc.2022.153987.
25. Makai L., Kalas B., Tiborcz G. Spectroscopic ellipsometry investigation of free liquid-liquid and liquid-air interfaces. *Thin Solid Films*. 2023. **764**. https://doi.org/10.1016/j.tsf.2022.139634.
26. Kondratenko O.S., Romanyuk V.R., Dmitruk N.L., Pinkovska M.B. Optical properties of surface metal-dielectric composites based on Si and SiO_2. *J. Nano- Electron. Phys.* 2018. **10**, Issue 1. P. 01018 (1–8). 10.21272/jnep.10(1).01018.
27. Johnson P.B., Christy R.W. Optical constants of the noble metals. *Phys. Rev. B*. 1972. **6**, No 12. P. 4370–4379. https://doi.org/10.1103/PhysRevB.6.4370.
28. Palik E.D. *Handbook of Optical Constants of Solids.* Academic Press, 1998.
29. Poperenko L.V., Yampolskiy A.L., Makarenko O.V. *et al.* Observation of surface-plasmon resonance in metal-dielectric thin films covered by graphene. *Nanosistemi, Nanomateriali, Nanotehnologii*. 2019. **17**, No 3. P. 473–482. https://doi.org/10.15407/nnn.17.03.473.
30. Christensen T., Yan W., Jauho AP. *et al.* Quantum corrections in nanoplasmonics: Shape, scale, and material. *Phys. Rev. Lett*. 2017. **118**. P. 157402. https://doi.org/10.1103/PhysRevLett.118.157402.
31. Jin D., Hu Q. Neuhauser D *et al.* Quantum-spillover-enhanced surface-plasmonic absorption at the interface of silver and high-index dielectrics. *Phys. Rev. Lett*. 2015. **115**. P. 193901. https://doi.org/10.1103/PhysRevLett.115.193901.
32. Giovannetti G., Khomyakov P.A., Brocks G. *et al.* Doping graphene with metal contacts. *Phys. Rev. Lett*. 2008. **101**. P. 026803. https://doi.org/10.1103/PhysRevLett.101.026803.
33. Khurgin J.B. Ultimate limit of field confinement by surface plasmon polaritons. *Faraday Discuss*. 2015. **178**. P. 109. https://doi.org/10.1039/C4FD00193A.
34. Rodríguez-de Marcos L.V., Larruquert J.I. Analytic optical-constant model derived from Tauc-Lorentz and Urbach tail. *Opt. Express*. 2016. **24**, No 25. P. 28561–28572. https://doi.org/10.1364/OE.24.028561.
35. Jellison G.E., Jr., Modine F.A. Parameterization of the optical functions of amorphous materials in the interband region. *Appl. Phys. Lett*. 1996. **69**, No 3. 371–373. https://doi.org/10.1063/1.118064.
36. Likhachev D.V., Malkova N., Poslavsky L. Modified Tauc–Lorentz dispersion model leading to a more accurate representation of absorption features below the bandgap. *Thin Solid Films*. 2015. **589**. P. 844–851. https://doi.org/10.1016/j.tsf.2015.07.035.
37. Budai J., Hanyecz I., Szilágyi E., Tóth Z. Ellipsometric study of Si_xC films: Analysis of Tauc–Lorentz and Gaussian oscillator models. *Thin Solid Films*. 2011. **519**. P. 2985–2988. https://doi.org/10.1016/j.tsf.2010.12.073.
38. Fodor B., Kozma P., Burger S. *et al.* Effective medium approximation of ellipsometric response from random surface roughness simulated by finite-element method. *Thin Solid Films*. 2016. **617**, pt A. P. 20–24. https://doi.org/10.1016/j.tsf.2016.01.054.
39. Liu Y., Qiu J., Liu L. Applicability of the effective medium approximation in the ellipsometry of randomly micro-rough solid surfaces. *Opt. Express*. 2018. **26**, Issue 13. P. 16560–16571. https://doi.org/10.1364/OE.26.016560.
40. Losurdo M., Hingerl K. (Eds) *Ellipsometry at the Nanoscale*. Springer, 2013.
41. Slovick B.A., Yu Z.G., Krishnamurthy S. Generalized effective-medium theory for metamaterials. *Phys. Rev. B*. 2014. **89**, No 15. P. 155118. https://doi.org/10.1103/PhysRevB.89.155118.
42. Arwin H., Aspnes D.E. Determination of optical properties of thin organic films by spectroellipsometry. *Thin Solid Films*. 1986. **138**, No 2. P. 195–207. https://doi.org/10.1016/0040-6090(86)90393-7.
43. Gorban N.Ya., Poperenko L.V. Optimized variant of the Beattie-Conn method in the study of the features of the optical properties of nickel in the visible region of the spectrum. *J. Appl. Spectrosc*. 1980. **33**. P. 1120–1124. https://doi.org/10.1007/BF00608389.

Authors' contributions

Kovanzhi P.O.: writing – original draft, methodology, project administration.
Hyrman I.H.: investigation, formal analysis.
Kravets V.G.: supervision, conceptualization, validation, writing – original draft.
Kondratenko O.S.: investigation, resources, formal analysis.
Poperenko L.V.: methodology, data curation, writing – review & editing.

Authors and CV

Petro O. Kovanzhi, PhD of the Department of Optics, Faculty of Physics, at the Taras Shevchenko National University of Kyiv. The area of scientific interests covers spectroellipsometry, optoelectronics, layered structures.
E-mail: petrk1695@gmail.com,
https://orcid.org/0000-0003-4681-3720

Ihor H. Hyrman, student of the Department of Optics, Faculty of Physics at the Taras Shevchenko National University of Kyiv. Field of research: ellipsometry, hetero-structures with noble metal inner layer.
E-mail: i.hyrman@gmail.com

Olga S. Kondratenko, PhD in Physics and Mathematics, Researcher at the Laboratory of Multi-angle spectroscopic ellipsometry at the V. Lashkaryov Institute of Semiconductor Physics, NAS of Ukraine. The area of scientific interests includes optoelectronics, plasmonics, optics, nanophotonics, thin films.
E-mail: kondratenko@isp.kiev.ua,
https://orcid.org/0000-0003-1948-4431

Vasyl G. Kravets received his PhD degree in physics (1990) from the Taras Shevchenko Kyiv State University. He worked at the Institute for Information Recording, NASU as a postdoctoral research scientist and later as a postdoctoral research fellow at the University of York, UK, and an invited research scientist at the University of Duisburg, Germany. Currently he is a Research Fellow in the plasmonic group of Prof. A. Grigorenko at the Department of Physics and Astronomy, the University of Manchester, UK. His current research interest focuses on development of hybrid plasmonic-two-dimensional nanostructures and their applications in biosensing, optoelectronic and solar photovoltaics field.
E-mail: Vasyl.Kravets@manchester.ac.uk,
https://orcid.org/0000-0003-1895-1106

Leonid V. Poperenko, Doctor of Science in Physics and Mathematics, Professor at the Department of Optics, Faculty of Physics, at the Taras Shevchenko National University of Kyiv. Authored over 200 publications, 14 patents, 5 textbooks. The area of scientific interests covers spectroscopic ellipsometry, ellipsometry, surface characterization, surface science, nanostructured materials, surface modification.
E-mail: plv@univ.kiev.ua,
https://orcid.org/0000-0003-4931-9066

Вплив провідності верхнього покриття на оптичні властивості тонких Cu(Ag)-шаруватих структур

П.О. Кованжі, І.Г. Гирман, В.Г. Кравець, О.С. Кондратенко, Л.В. Поперенко

Анотація. У роботі вивчаються оптичні властивості тонких Cu (Ag)-шаруватих структур, покритих захисними шарами на основі оксидів графену, титану (TiO_2) або алюмінію (Al_2O_3). Мета роботи полягає в дослідженні впливу цих покриттів на оптичну поведінку металевих плівок, що знаходяться під ними, зокрема в спектральному діапазоні збудження поверхневих плазмонних резонансів. Для аналізу оптичних характеристик гібридних метал-оксид-графенових плівок використано комбіновані методи спектрорефлектометрії та спектроеліпсометрії. Дослідження показує, що графен завдяки своїй надзвичайній електропровідності та унікальним оптоелектронним властивостям значно змінює оптичну поведінку досліджуваних структур. Це включає помітні зміни в показниках заломлення та поглинання, а також оптичної провідності, що вказує на можливість підсилення взаємодії світло-речовина в плазмонно-графенових шаруватих структурах з метою застосування як біосенсора. Важливо, що додавання шарів TiO_2 і Al_2O_3 також сильно впливає на оптичні властивості, які мають відношення до їх відповідних застосувань у галузях оптоелектроніки та мікроелектроніки. Використання наближення ефективного середовища та моделі Тауца–Лоренца сприяє глибшому розумінню взаємодії між міжзонним і внутрішньозонним електронним переходом на нанорозмірному рівні. Було виявлено, що товщина шару створених матеріалів та їхні окремі діелектричні функції разом із додаванням моношару графену значно змінюють оптичні властивості гібридних шаруватих структур. Отримані результати є важливими для галузей плазмоніки та нанотехнологій, надаючи ідеї для розробки сенсорів і пристроїв з покращеними оптичними характеристиками.

Ключові слова: оптика тонких шарів, графенові покриття, спектроеліпсометрія, плазмоніка, застосування у біосенсориці.